Prompt gamma rays induced by inelastic scattering of fission neutrons on iron

Zeljko Ilic[1,2] · Eric Mauerhofer[1] · Christian Stieghorst[3] · Zsolt Révay[3] · Matthias Rossbach[4] ·
Tsitohaina H. Randriamalala[1] · Thomas Brückel[1,2]

Abstract

Prompt gamma rays induced by (n,n′γ) reactions on iron were measured with the instrument FanGaS (Fast Neutron induced Gamma-Ray Spectrometry) operated at the Heinz Maier-Leibnitz Zentrum (MLZ) in Garching. The measurement was performed at an angle of 90° between neutron beam and detector. The fast neutron flux at the sample position was determined to be 1.40×10^8 cm^{-2} s^{-1} by using the foil activation method. Energies, relative intensities and fast neutron spectrum averaged isotopic cross section for production of 81 prompt gamma lines are presented. The results obtained are found in good agreement with literature data. The new set of gamma lines is recommended to replace the old dataset with several new lines also recognizing a few false identifications. This work is an important step towards the future chemical analysis of large samples at FanGaS employing highly penetrating fission neutrons.

Keywords Fast neutrons · Iron · Inelastic scattering · Prompt gamma ray · Cross section

Introduction

Accurate non-destructive chemical analysis of materials is of fundamental importance in many fields of science and for industrial applications. Prompt Gamma Neutron Activation Analysis (PGNAA) based on cold/thermal neutron capture is well established as a powerful non-destructive analytical technique to determine the elemental composition of small and thin samples [1]. Large objects may be investigated to some extent by PGNAA using cold or thermal neutron beams [2–4]. Nevertheless, depending on the neutron absorption properties of the sample, the penetration depth of cold/thermal neutrons is limited and the beam attenuation must be corrected for [4, 5]. Therefore, neutrons of higher energies are a better choice for the analysis of large and thick objects. Unlike cold/thermal neutrons inducing (n, γ) reactions, high-energy neutrons induce other reactions, particularly (n,n′) or (n,p), (n,α) or even (n,2n) in some cases. Cross sections for these reactions are generally lower compared to thermal neutron capture reactions. However, as capture cross sections outside nuclear resonances follow a 1/v trend (v being the neutron velocity), at higher energies e.g. at 2 MeV mean energy of fission neutrons, inelastic scattering with the emission of isotope-specific prompt gamma rays prevail.

The possibility to determine the elemental composition of large samples by measuring prompt gamma rays with a NaI(Tl) detector following the inelastic scattering of 14-MeV pulsed neutrons for remote analysis of surfaces was reported first in 1961 by Schrader and Stinner [6]. In 1976, Jiggins and Habbani [7] used 3.29 MeV neutrons, produced by the ^{2}H(d,n)^{3}He reaction, for the determination of iron in iron ores measuring prompt gamma rays with a NaI(Tl) detector and presented analytical sensitivities for 23 elements. Two years later, Yates et al. [8] proposed a time-of-flight method based on neutron/gamma coincidence to improve sensitivity of prompt gamma-ray detection with a Ge(Li) detector rejecting background signals induced by scattered neutrons. The method was applied to the analysis of metal alloys using 2.5 MeV neutrons and limits of detection for 38 elements

✉ Eric Mauerhofer
e.mauerhofer@fz-juelich.de

1 Jülich Centre for Neutron Science, Forschungszentrum Jülich GmbH, 52425 Jülich, Germany

2 Lehrstuhl für Experimentalphysik IVc, RWTH Aachen University, 52056 Aachen, Germany

3 Heinz Maier-Leibnitz Zentrum (MLZ), Technische Universität München, Lichtenbergstr, 85748 Garching, Germany

4 Kreuzau, Germany

were determined. In 1979, Sowerby [9] investigated the use of isotopic neutron sources for elemental analysis of kilogram samples by neutron inelastic scattering associated gamma rays. These preliminary works have resulted in the following years till now to the development of various laboratories, in situ or online techniques using either isotopic neutron sources or neutron generators and mainly scintillation detectors (NaI(Tl), BGO or LaBr$_3$) for bulk analysis (well and bore-hole logging, process and quality control of materials such as coal, cement and ores) or for detection of explosive and illicit materials. However, due to the low fast neutron flux delivered by these sources and the poor resolution of the employed detectors, the analytical sensitivity of the developed techniques is limited to few % per sample weight. Therefore, it was decided to use the intense fission neutron beam delivered by the SR10 (Strahlrohr 10) channel of the research reactor FRM II (Forschungs-Neutronenquelle Heinz-Maier-Leibnitz) for accurate analysis of large samples measuring prompt gamma rays induced by inelastic scattering of fission neutrons.

Compared to the well documented thermal neutron prompt gamma spectra and associated energies [1], a tabulation of prompt gamma energies and associated relative intensities induced by fission neutrons of all elements has been published only once in 1978 by Demidov et al. [10]. The measurements were performed at the Baghdad Nuclear Research Institute, while the evaluation has been carried out at the Kurchatov Institute, Moscow. A fission neutron beam (filtered with 9 cm of lead, 1 cm boron carbide and 1 mm of cadmium) with the diameter of 3 cm was used for the irradiation. The gamma rays emitted by the sample under 90 degrees were filtered using 8 cm of LiH and acquired by a 30-cm^3 (equivalent to 10% relative efficiency) Ge(Li) detector. The detector was shielded with 5 cm iron, 8 cm boron carbide-loaded paraffin, 10 cm of lead, and 3 mm of ^{6}Li. This pioneering work covering a reasonable range of gamma-ray energies is valuable. However, the energy resolution of the Ge(Li) detector was degrading after an extended neutron exposure. Thus, to perform precise chemical analysis of samples with fission neutrons a comprehensive data catalogue on (n,n′γ) reactions, prompt gamma-ray energies and absolute intensities is urgently needed. Furthermore, these data may help in the development of nuclear data libraries that serve a multitude of applications.

To achieve this, the FaNGaS (Fast Neutron induced Gamma Spectrometry) instrument [11, 12] has been designed and installed at the MEDAPP (Medical Application) [13] facility of FRM II (Fig. 1). The first characterization of FaNGaS and the neutron spectrum at sample position is given in [11]. In this work, the fast neutron spectrum and flux at sample position is determined again due to a modification of the fast neutron collimation. The results obtained from the measurement of prompt gamma rays induced by
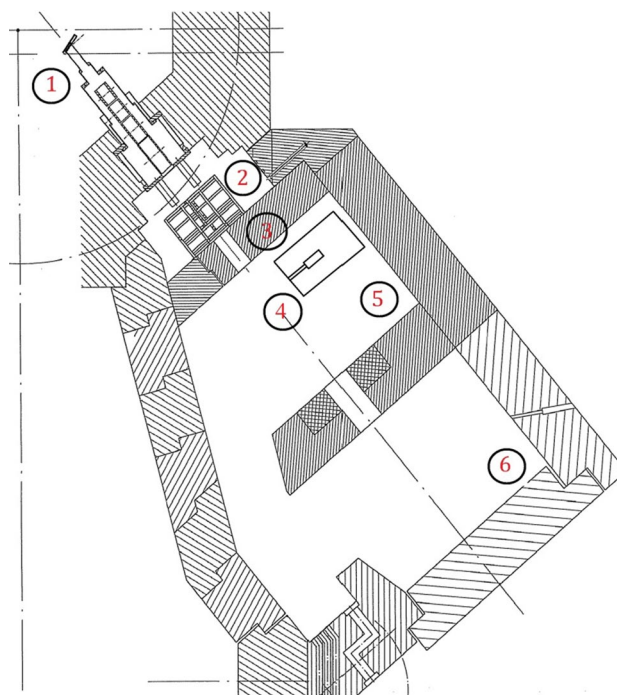

Fig. 1 Schematic view of the fast neutron facility at FRM II. (1) convertor plate made of 498 g of highly enriched uranium (93% of ^{235}U) plunged into the reactor pool at at disatnce of about 1 m for the reactor core; (2) bench filters bunker containing the collimator of FaNGaS instrument; (3) mutli-leaf-collimator of the MEDAPP facility; (4) FaNGaS spectrometer at measuring position; (5) bunker of the MEDAPP facility; (6) bunker of the NECTAR facility

inelastic scattering of fission neutrons on iron at an angle of 90° between the neutron beam and the detector are presented and compared to literature data.

FaNGaS instrument

In the first version of the FaNGaS instrument the collimation of fast neutrons was achieved using a set of two collimators made of polyethylene, boron carbide and lead. The inner collimator was placed inside the filter bench room while the outer collimator was positioned in the opening of the multi-leaf-collimator of the irradiation facility MEDAPP inside the biological shield. Technical details and dimensions of the collimators are given in [11]. Due to the upgrade of the fast neutron imaging facility NECTAR (Neutron Computerized Tomography and Radiography) to perform radiography or tomography also with thermal neutrons [14], the filter set-ups inside the filter bench room have been modified and the FaNGaS outer collimator was removed from the MEDAPP multi-leaf-collimator. In order to filter thermal neutrons from the fast neutron beam and to attenuate gamma radiation coming from the reactor, a boron carbide plate with a thickness of 1 cm and two lead plates with a total thickness of 5 cm

were placed at the upstream beam side of the inner collimator (see Fig. 2). Due to these changes, a new determination of the fast neutron flux at sample position was necessary.

In addition, the shielding of the HPGe-detector was also partially modified. In order to increase thermal neutron absorption, the 30 cm thick polyethylene layers at the front side of the shielding have been replaced by borated polyethylene of same thickness. For gamma-ray collimation, a removable cylindrical lead collimator with 6 cm inner diameter, 2 cm wall thickness and 16 cm length was inserted into the cylindrical aperture (10 cm diameter) of the front shielding. The detector set up at experimental position is shown in Fig. 2.

Neutron flux determination

The fast neutron spectrum in the energy range 0.075–20 MeV at the sample position was determined by means of the foil activation technique. High-purity foils of various elements (Al, Ti, Fe, Ni, Zr and In) were sealed in Teflon bags and irradiated separately for 8–18 h. The dimension of the foils is about $25 \times 25 \times 0.25$ mm^3. After irradiation, the gamma-ray spectra of the activated foils were measured at a distance of 17 cm from the HPGe-detector. The counting times ranged from 2 to 21 h. The gamma-ray spectra were analyzed with the HYPERMET-PC software [15]. The reaction rates, R, for neutron spectrum unfolding were calculated using the following relation:

$$R = \frac{\ln 2 \cdot P_{E\gamma}}{\varepsilon_{E\gamma} \cdot I_{E\gamma} \cdot T} \cdot \frac{e^{\frac{\ln 2 \cdot t_d}{T}}}{\left(1 - e^{\frac{-\ln 2 \cdot t_i}{T}}\right) \cdot \left(1 - e^{\frac{-\ln 2 \cdot t_c}{T}}\right)} \quad (1)$$

where $P_{E\gamma}$ is the net count for the gamma-ray of energy $E\gamma$, $\varepsilon_{E\gamma}$ is the full-energy-peak efficiency at measuring position determined in [11], $I_{E\gamma}$ the gamma emission probability, T is the half-life of the activation product, t_i is the irradiation time, t_c is the counting time and t_d the decay time, i.e. the time between end of irradiation and beginning of the counting. Corrections for neutron and gamma absorption were neglected since the foils are very thin. The masses of the foils, the investigated reactions and the calculated reactions rates per atom are given in Table 1.

The software suit STASYL PNNL was used for neutron spectrum unfolding [16]. This code provides a solution for the neutron spectrum using the generalized least-square method. Detailed information about the method can be found in [17]. The code takes as input the reaction rates and a predefined neutron spectrum divided into a certain number of energy groups. For the purpose of this work, the neutron spectrum previously determined with the initial setup of neutron collimators was used as an input and the number of energy groups was set to 100. The obtained neutron spectrum is compared with the previous one determined with the former set of neutron collimators in Fig. 3. A relatively higher average neutron energy of 2.30 MeV and a fast neutron flux $(1.40 \pm 0.05) \times 10^8$ cm^{-2} s^{-1} were obtained due to the removal of the outer collimator from the MEDAPP

Fig. 2 The left piture shows detector setup at experimental position: (1) the front side of the MEDAPP multi-leaf neutron beam collimator; (2) front shielding made of borated polyethylene; (3) detector collimator; (4) sample holder made of Teflon; (5) iron support frame. The upper right picture shows the inner neutron collimator on the filter bench. The down right picture shows the boron carbide and lead filters in front of the neutron collimator
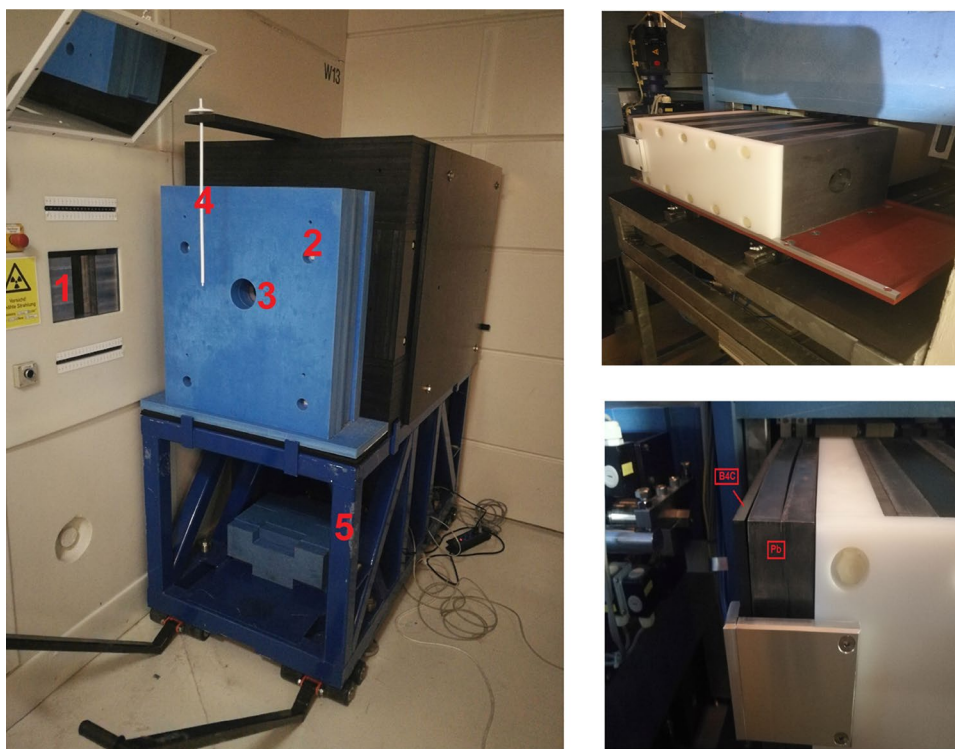
Table 1 List of irradiated foils with their respective masses, investigated reactions with their corresponding threshold energies, E_{thr} [11], considered gamma-rays energy, $E\gamma$, and determined reaction rates, R

Element	Mass (g)	Reaction	E_{thr} (MeV)	$E\gamma$ (keV)	R (atom^{-1} s^{-1})	σ (mb)	$\sigma_{fission}$ (mb)
Al	0.343	^{27}Al(n,p)^{27}Mg	1.896	843	$(6.22\pm0.14)\times10^{-19}$	4.44 ± 0.18	4.32 ± 0.16
		^{27}Al(n,α)^{24}Na	3.249	1368	$(1.46\pm0.04)\times10^{-19}$	1.04 ± 0.05	0.88 ± 0.02
Ti	0.772	^{47}Ti(n,p)^{47}Sc	0.075	159	$(2.83\pm0.07)\times10^{-18}$	20 ± 1	18.3 ± 0.6
		^{48}Ti(n,p)^{48}Sc	3.276	1037	$(6.40\pm0.35)\times10^{-20}$	0.46 ± 0.03	0.37 ± 0.03
Fe	1.282	^{56}Fe(n,p)^{56}Mn	2.965	846	$(1.94\pm0.02)\times10^{-19}$	1.39 ± 0.05	1.27 ± 0.02
Ni	2.806	^{58}Ni(n,p)^{58}Co	0.49	811	$(1.88\pm0.03)\times10^{-17}$	134 ± 5	108 ± 1
Zr	1.109	^{90}Zr(n,2n)^{89}Zr	12.1	909	$(1.93\pm0.66)\times10^{-20}$	0.138 ± 0.05	0.170 ± 0.05
In	1.334	^{115}In(n,n')^{115m}In	0.339	336	$(2.89\pm0.03)\times10^{-17}$	206 ± 7	188 ± 11[a]
In	1.334	^{115}In(n,γ)^{116m}In	–	1097, 1293	$(5.63\pm0.08)\times10^{-17}$	–	–

σ is the neutron spectrum averaged cross section of the reaction. $\sigma_{fission}$ is the cross section evaluated for a fission spectrum ($kT = 1.35$ MeV) in JANIS (mean value from various nuclear data libraries) [18]

[a]Value taken in Ref. [25]

Fig. 3 Energy spectra of the incident neutron beam of FaN-GaS at sample position. Orange histogram (a): determined in the energy range 10^{-8} to 20 MeV using the inner and outer neutron collimators [11]. Green histogram (b): determined in the energy range 0.075–20 MeV using the inner neutron collimator with B_4C and Pb filters (this work). The zoom in the figure shows the energy spectra for the fast neutron region
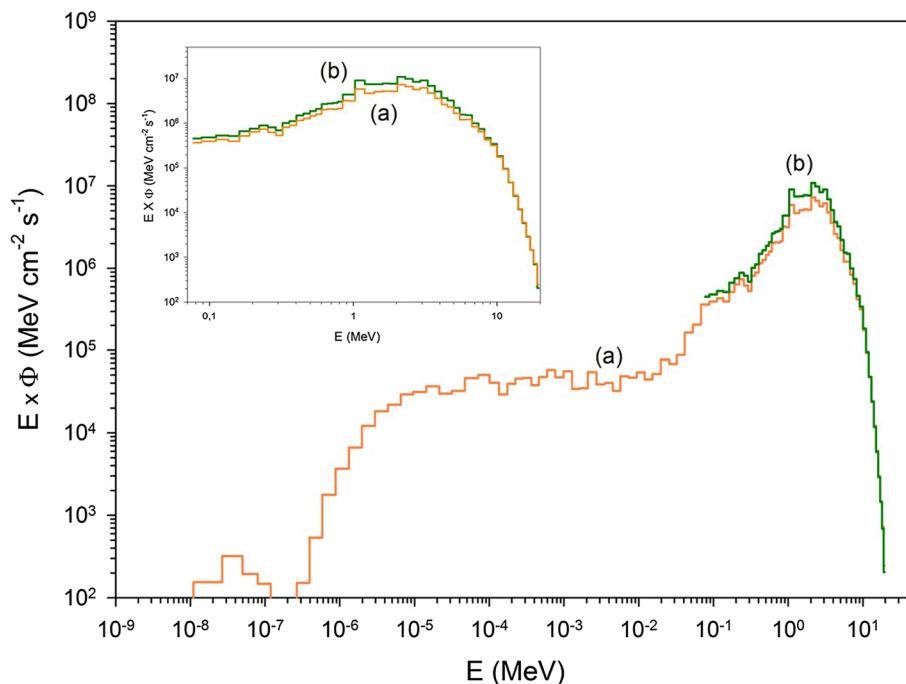
multi-leaf-collimator. The fast neutron spectrum averaged cross sections were determined according to $\sigma = R/\Phi$, for the threshold reactions listed in Table 1. The results compare well with the values evaluated for a fission spectrum ($kT = 1.35$ MeV) given in JANIS (Java-based Nuclear Data Information System) Book of neutron induced cross section [18] (see Table 1). The differences may be related to the deviation of the fast neutron spectrum from a Watt spectrum.

The neutron flux in the energy range 10^{-8}–0.075 MeV was not determined in this work since these neutron energies are not expected to contribute significantly to the inelastic channel. As shown in Fig. 3 (orange histogram, (a)), the neutron flux integrated over this region (mainly resonance neutrons) represents only 2% of the total neutron flux. Here, we may suppose that the resonance neutron flux is almost the same since the rate measured for the reaction ^{115}In(n,γ)^{116m}In, $(5.63\pm0.08)\times10^{-17}$ atom^{-1} s^{-1}, is close to the value measured in [11], $(5.03\pm0.08)\times10^{-17}$ atom^{-1} s^{-1}. (Color figure online)

Prompt gamma rays of iron

The gamma-ray spectrum of the iron foil ($m = 1.282$ g) was recorded during irradiation. The measurement was performed at an angle of 90° with respect to the neutron beam

direction. The gamma lead-collimator was used. The distance between foil and detector was 67 cm. The iron foil of natural composition was irradiated and counted for 10 h (live time was 7.6 h). To support the identification of the prompt gamma lines, a beam background (i.e. irradiation without sample) was also recorded for 12.9 h. The spectra were analyzed with the software HYPERMET-PC [15]. The gamma-ray spectra are shown together for various energy ranges in Figs. 4, 5, and 6. The identified isotopes with the

associated gamma-ray energies are given in the spectra; those with asterisks belong to the beam background. The latter contains prompt and delayed gamma rays induced by fast neutron interaction or neutron capture with the HPGe detector (Ge, Al, Cu, In), the shielding (B, H, Pb), the supporting frame (Fe), the sample holder made of Teflon (F) and the air (N, O). It was also seen that when the lead collimator was close to the detector, the boron peak at 478 keV is fully suppressed (Fig. 4) and the count rate of the 2223 keV

Fig. 4 Gamma-ray spectra in the energy range 0–2000 keV recorded during 27,330 s for the iron foil (red) and during 46,454 s for the active background (black). Background gamma rays are marked with asterisks. Prompt gamma-rays of iron are written in bold. Abbreviations SE and DE stand for single and double escape peak (color figure online)

Fig. 5 Gamma-ray spectra in the energy range 2000–4000 keV recorded during 27,330 s for the iron foil (red) and during 46,454 s for the active background (black). Background gamma rays are marked with asterisks. Prompt gamma-rays of iron are written in bold. Abbreviations SE and DE stand for single and double escape peak (color figure online)
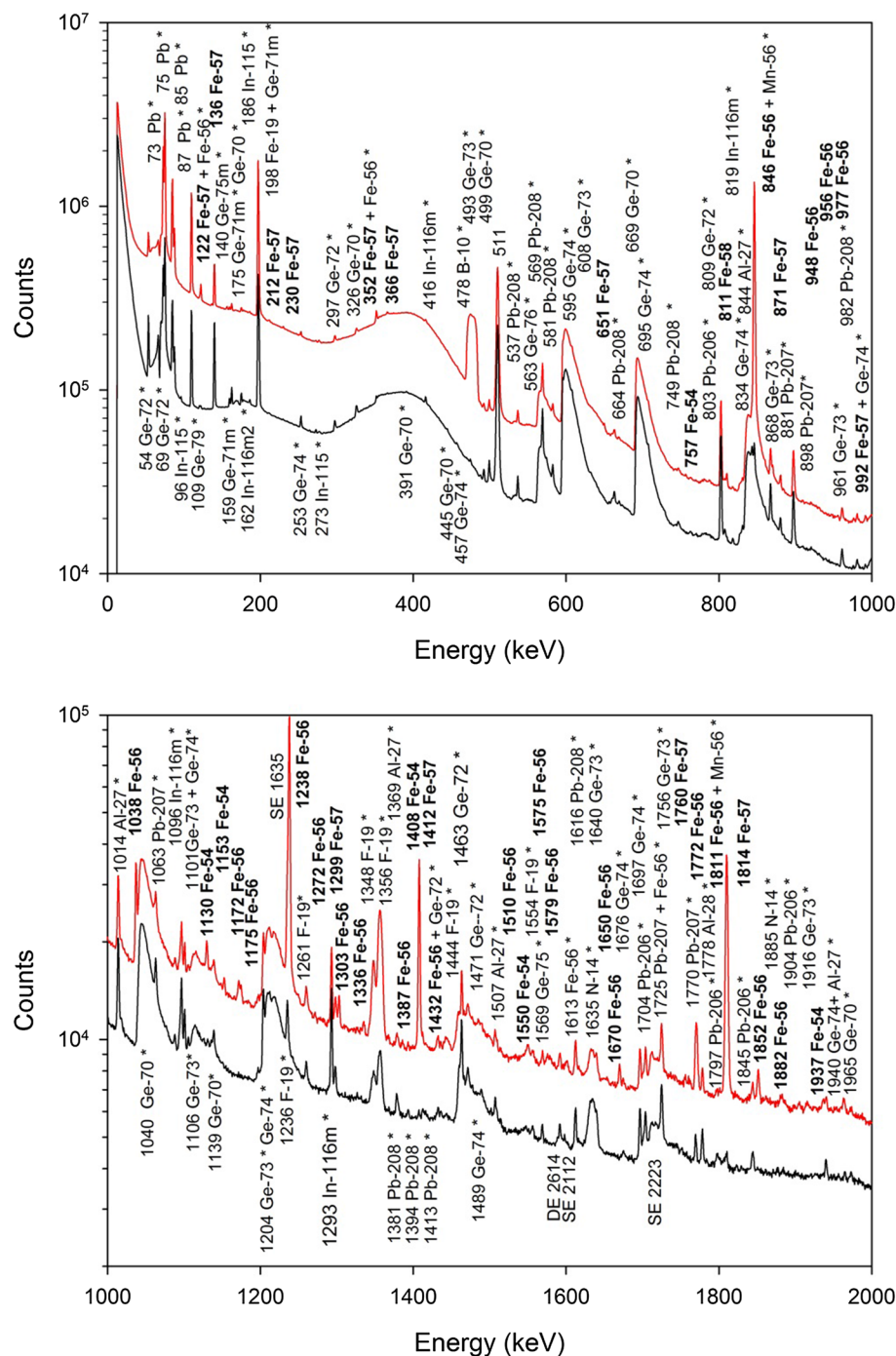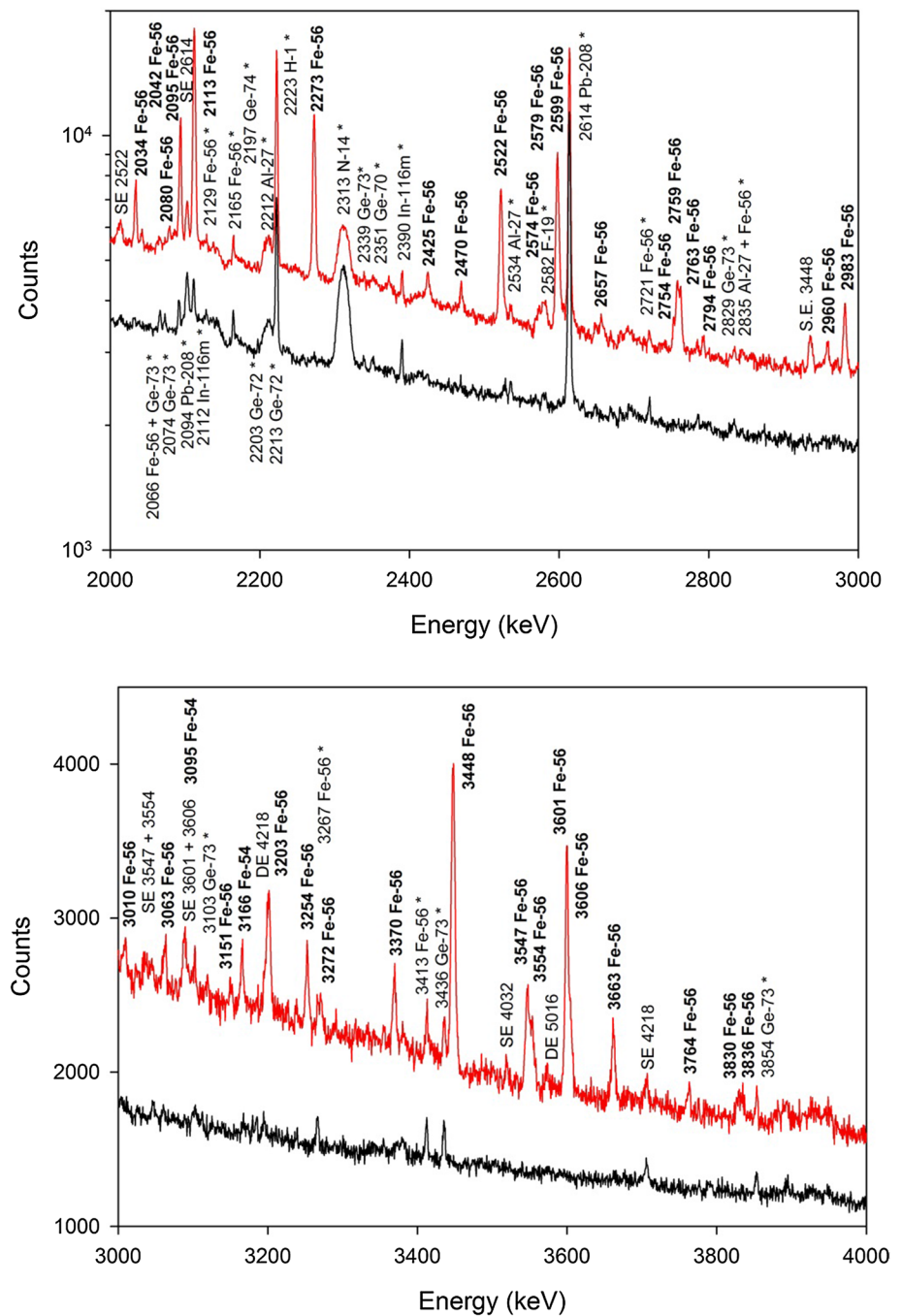

hydrogen gamma line is reduced by a factor of about 3, both gamma rays being mainly produced in the front shielding.

Besides background lines, the spectrum of the iron contains the most intense prompt gamma rays induced by the inelastic scattering of fast neutrons on the iron isotopes ^{54}Fe, ^{56}Fe, ^{57}Fe and ^{58}Fe. Gamma lines of ^{19}F also appear due to the sample packing made of Teflon. In comparison to the beam background, the count rates of lines attributed to the background are higher in the iron spectrum by a mean factor of 1.32 ± 0.05 due to neutrons scattered by the sample

towards the detector. This factor was used to correct for the background interferences. The iron gamma rays were assigned to specific nuclear transitions of an iron isotope based on the database NuDat 2.8 [19]. Contributions from (n,p) and (n,α) reactions were neglected due to their low cross sections compared to the (n,n′) reaction. A total of 81 prompt gamma lines of iron were identified, 59 associated to ^{56}Fe, 12 to ^{57}Fe, 9 to ^{54}Fe and 1 to ^{58}Fe (see Tables 2, 3, 4). Compared to the work of Demidov et al. [10], additional gamma lines were also detected (23 for ^{56}Fe, 7 for ^{57}Fe and 3

Fig. 6 Gamma-ray spectra in the energy range 4000–8000 keV recorded during 27,330 s for the iron foil (red) and during 46,454 s for the active background (black). Background gamma rays are marked with asterisks. Prompt gamma-rays of iron are written in bold. Abbreviations SE and DE stand for single and double escape peak (color figure online)
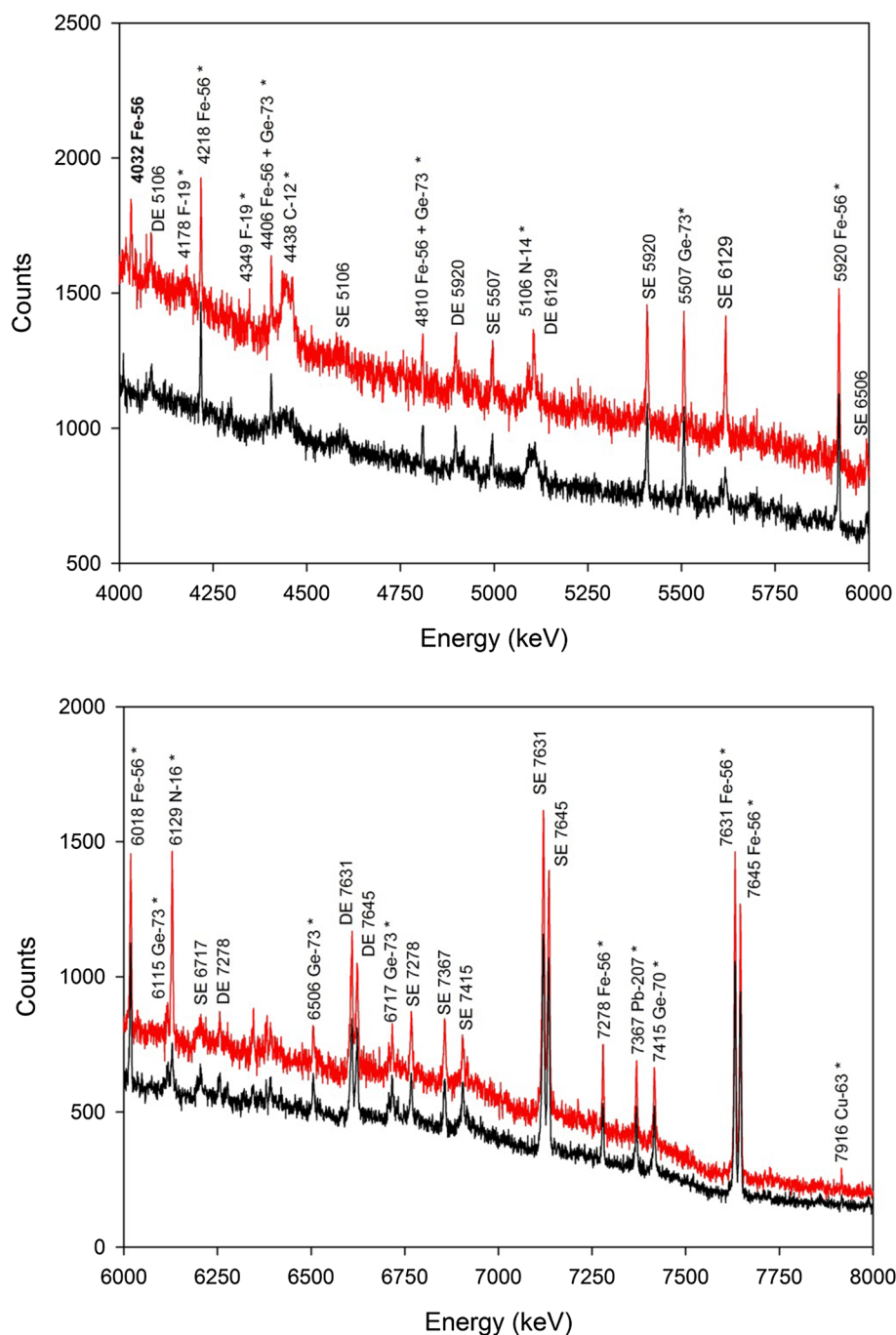
for ^{54}Fe) due to the better resolution of our detector (2.1 keV vs. 3.8 keV for the detector used in [10]). On the other hand, 13 gamma lines listed at energies 1213.0, 1359.9, 1454.5, 1528.6, 1612.2, 1725.6, 1760.8, 2211.7, 2027.0, 2062.4, 2192.9, 3634.9 and 4541.7 keV in the Demidov Atlas were not observed. The line at 1359.9 keV could not be uniquely identified due the Doppler broadening of the 1356.5 keV line of ^{19}F induced by interaction of fission neutrons with Teflon. It was not possible to observe the lines at 1612.2 and 1725.6 keV, respectively, due to interferences of the

1612.8 keV line of ^{56}Fe produced by thermal neutron capture of the iron frame and of the 1726.5 keV line of ^{207}Pb induced by inelastic scattering of fast neutrons with lead, respectively. Also, the line at 2211.7 keV was not identified due to interference of the line at 2211.8 keV of ^{27}Al issued from the inelastic scattering of fast neutrons with the aluminum cap of the detector. The remaining gamma rays which are not mentioned in the database NuDat 2.8 are probably assigned spuriously to iron in the Demidov Atlas, their intensities being measured with uncertainties as large as 50% in some

Table 2 Prompt gamma rays of ^{56}Fe

This work				From Demidov Atlas [10]		I_R (this work)/I_R (Demidov)
$E\gamma$ (keV)	$P_{E\gamma}(90°)/\varepsilon_{E\gamma}$ $(\times 10^{-8})$ (count)	I_R (relative) (%)	$\langle\sigma_{E\gamma}(90°)\rangle$ (mb)	$E\gamma$ (keV)	I_R (relative) (%)	
846.86 ± 0.04	284 ± 17	100	586 ± 41	846.78	100	1
948.3 ± 0.3	0.21 ± 0.05	0.07 ± 0.02	0.43 ± 0.10	–	–	–
956.1 ± 0.2	0.33 ± 0.06	0.12 ± 0.02	0.67 ± 0.13	–	–	–
976.8 ± 0.2	0.18 ± 0.05	0.06 ± 0.02	0.37 ± 0.10	–	–	–
1037.81 ± 0.05	5.17 ± 0.27	1.82 ± 0.14	10.7 ± 0.7	1037.85	2.15 ± 0.10	0.85 ± 0.08
1172.15 ± 0.09	0.74 ± 0.05	0.26 ± 0.02	1.5 ± 0.1	1173.2 ± 0.8	0.25 ± 0.10	1.04 ± 0.42
1175.1 ± 0.1	0.58 ± 0.05	0.20 ± 0.02	1.2 ± 0.1	1175.0 ± 0.8	0.15 ± 0.10	1.33 ± 0.90
1272.1 ± 0.5	0.19 ± 0.05	0.07 ± 0.02	0.40 ± 0.10	1271.9 ± 0.1	0.05 ± 0.02	1.40 ± 0.70
1238.30 ± 0.05	28 ± 2	9.90 ± 0.92	58 ± 5	1238.3 ± 0.2	10.5 ± 0.5	0.94 ± 0.10
1303.52 ± 0.07	0.93 ± 0.07	0.33 ± 0.03	1.9 ± 0.2	1303.2 ± 0.3[a]	0.64 ± 0.10	0.52 ± 0.09
1335.7 ± 0.2	0.4 ± 0.07	0.14 ± 0.02	0.8 ± 0.1	1334.6 ± 0.4	0.18 ± 0.03	0.78 ± 0.17
1386.6 ± 0.4	0.23 ± 0.03	0.08 ± 0.01	0.48 ± 0.07	1386.6 ± 1.0	0.06 ± 0.03	1.33 ± 0.69
1432.5 ± 0.2	0.17 ± 0.03	0.06 ± 0.01	0.35 ± 0.07	1434.2 ± 0.1	0.05 ± 0.02	1.20 ± 0.52
1575.8 ± 0.2	0.23 ± 0.03	0.08 ± 0.01	0.47 ± 0.07	–	–	–
1579.5 ± 0.2	0.18 ± 0.03	0.06 ± 0.01	0.36 ± 0.07	–	–	–
1650.4 ± 0.5	0.23 ± 0.04	0.08 ± 0.01	0.49 ± 0.09	1650.8 ± 0.09	0.09 ± 0.03	0.89 ± 0.31
1670.7 ± 0.1	0.54 ± 0.05	0.19 ± 0.02	1.1 ± 0.1	1671.1 ± 0.6[b]	0.32 ± 0.05	0.59 ± 0.11
1771.7 ± 0.1	1.48 ± 0.13	0.52 ± 0.05	3.1 ± 0.3	1771.33[c]	0.91 ± 0.08	0.57 ± 0.07
1810.77 ± 0.05	18 ± 1	6.32 ± 0.59	37 ± 3	1810.5 ± 0.2	6.9 ± 0.5	0.92 ± 0.11
1852.00 ± 0.07	0.83 ± 0.06	0.29 ± 0.03	1.7 ± 0.2	1851.8 ± 0.3	0.39 ± 0.06	0.74 ± 0.14
1882.3 ± 0.4	0.34 ± 0.03	0.12 ± 0.01	0.70 ± 0.07	1882.6 ± 0.3	0.33 ± 0.05	0.36 ± 0.06
2015.1 ± 0.2	0.49 ± 0.06	0.17 ± 0.02	1.0 ± 0.1	2015 ± 2	0.15 ± 0.08	1.13 ± 0.62
2034.66 ± 0.06	1.58 ± 0.13	0.56 ± 0.06	3.3 ± 0.3	2034.8 ± 0.3	0.46 ± 0.07	1.22 ± 0.23
2042.9 ± 0.2	0.30 ± 0.04	0.11 ± 0.02	0.62 ± 0.09	–	–	–
2079.9 ± 0.2	0.26 ± 0.04	0.09 ± 0.01	0.53 ± 0.08	–	–	–
2094.70 ± 0.06	3.40 ± 0.25	1.20 ± 0.11	7.0 ± 0.6	2094.6 ± 0.2	1.08 ± 0.07	1.11 ± 0.12
2113.11 ± 0.07	8.83 ± 0.63	3.10 ± 0.29	18 ± 1	2112.9 ± 0.2	3.2 ± 0.2	0.97 ± 0.11
2273.41 ± 0.06	5.56 ± 0.44	1.95 ± 0.19	11 ± 1	2273.2 ± 0.2	2.03 ± 0.12	0.96 ± 0.11
2372.6 ± 0.5	0.23 ± 0.04	0.08 ± 0.02	0.47 ± 0.09	2372.2 ± 0.07	0.09 ± 0.03	0.89 ± 0.37
2425.5 ± 0.1	0.57 ± 0.06	0.20 ± 0.02	1.2 ± 0.1	–	–	–
2470.2 ± 0.2	0.43 ± 0.11	0.15 ± 0.04	0.9 ± 0.2	–	–	–
2522.42 ± 0.09	4.34 ± 0.37	1.53 ± 0.16	9.0 ± 0.8	2523.2 ± 0.2	1.28 ± 0.10	1.20 ± 0.16
2574.4 ± 0.2	0.46 ± 0.06	0.16 ± 0.02	0.9 ± 0.1	–	–	–
2579.2 ± 0.2	0.33 ± 0.06	0.12 ± 0.02	0.7 ± 0.1	–	–	–
2598.9 ± 0.2	3.65 ± 0.37	1.28 ± 0.15	7.5 ± 0.8	2598.52	2.6 ± 0.2	0.49 ± 0.07
2657.0 ± 0.3	0.45 ± 0.06	0.16 ± 0.02	0.9 ± 0.1	2658.3 ± 0.8	0.14 ± 0.04	1.14 ± 0.36
2754.5 ± 0.2	0.56 ± 0.06	0.20 ± 0.02	1.2 ± 0.1	–	–	–
2759.1 ± 0.1	1.4 ± 0.1	0.50 ± 0.05	2.9 ± 0.3	2760.0 ± 0.3[f]	1.24 ± 0.10	0.40 ± 0.05
2763.4 ± 0.1	1.2 ± 0.1	0.44 ± 0.05	2.6 ± 0.3	–	–	–
2793.9 ± 0.3	0.22 ± 0.04	0.08 ± 0.02	0.45 ± 0.09	–	–	–
2959.7 ± 0.2	0.43 ± 0.06	0.15 ± 0.02	0.9 ± 0.1	2959.6 ± 0.6	0.20 ± 0.04	0.75 ± 0.18
2983.2 ± 0.1	1.4 ± 0.1	0.50 ± 0.05	2.9 ± 0.3	2983.7 ± 0.6	0.46 ± 0.7	1.09 ± 0.20
3010.0 ± 0.4	0.23 ± 0.04	0.08 ± 0.02	0.47 ± 0.09	–	–	–
3063.6 ± 0.3	0.34 ± 0.05	0.12 ± 0.02	0.7 ± 0.1	–	–	–
3151.6 ± 0.4	0.19 ± 0.04	0.07 ± 0.01	0.38 ± 0.08	–	–	–
3202.8 ± 0.2	0.93 ± 0.12	0.33 ± 0.05	1.9 ± 0.3	3202.18[d]	0.78 ± 0.13	0.42 ± 0.02
3253.8 ± 0.2	0.68 ± 0.06	0.24 ± 0.03	1.4 ± 0.1	3253.7 ± 0.6	0.36 ± 0.7	0.67 ± 0.13

Table 2 (continued)

This work				From Demidov Atlas [10]		I_R (this work)/I_R (Demidov)
$E\gamma$ (keV)	$P_{E\gamma}(90°)/\varepsilon_{E\gamma}$ ($\times 10^{-8}$) (count)	I_R (relative) (%)	$\langle\sigma_{E\gamma}(90°)\rangle$ (mb)	$E\gamma$ (keV)	I_R (relative) (%)	
3272.6 ± 0.3	0.28 ± 0.04	0.10 ± 0.02	0.58 ± 0.09	3272.6 ± 1.0^e	0.17 ± 0.04	0.59 ± 0.18
3370.2 ± 0.2	0.62 ± 0.06	0.22 ± 0.03	1.3 ± 0.1	3369.2 ± 0.8	0.24 ± 0.05	0.92 ± 0.23
3447.7 ± 0.3	1.9 ± 0.3	0.68 ± 0.10	4.0 ± 0.5	3448.6 ± 0.4	1.13 ± 0.20	0.62 ± 0.14
3547.5 ± 0.2	0.94 ± 0.13	0.33 ± 0.05	1.9 ± 0.3	3548.5 ± 0.5 ^{g}	0.65 ± 0.16	0.51 ± 0.15
3554.1 ± 0.4	0.56 ± 0.06	0.20 ± 0.02	1.2 ± 0.1	–	–	–
3600.7 ± 0.2	2.5 ± 0.3	0.86 ± 0.10	5.1 ± 0.6	3601.9 ± 0.3 ^{h}	1.5 ± 0.3	0.60 ± 0.14
3606.0 ± 0.2	0.75 ± 0.13	0.27 ± 0.05	1.6 ± 0.3	–	–	–
3662.9 ± 0.3	0.76 ± 0.13	0.27 ± 0.05	1.6 ± 0.3	3663.1 ± 0.6	0.43 ± 0.14	0.63 ± 0.24
3763.7 ± 0.4	0.27 ± 0.04	0.10 ± 0.02	0.56 ± 0.09	–	–	–
3828.1 ± 0.5	0.25 ± 0.04	0.09 ± 0.02	0.52 ± 0.09	–	–	–
3833.8 ± 0.5	0.23 ± 0.04	0.08 ± 0.02	0.48 ± 0.09	–	–	–
4032.4 ± 0.3	0.38 ± 0.01	0.13 ± 0.01	0.79 ± 0.03	–	–	–

$E\gamma$ is the gamma-ray energy, $P_{E\gamma}(90°)/\varepsilon_{E\gamma}$ the net count in the gamma ray peak divided by the full-energy-peak efficiency, I_R the relative intensity of the gamma ray and $\langle\sigma_{E\gamma}(90°)\rangle$ the fast neutron spectrum averaged isotopic cross section for gamma ray production at angle of 90° between neutron beam and detector determined with Eq. (2)

Possible interference from [a] the 1298 keV line of ^{57}Fe; [b] the 1676 keV line of ^{74}Ge; [c] the 1770 keV line of ^{207}Pb; [d] the double escape peak of the 4218 keV line, [e] affected by the 3267 keV neutron capture line of ^{56}Fe. Not resolved doublet: [f] 2759 and 2764 keV; [g] 3547 and 3554 keV; [h] 3601 and 3606 keV

Table 3 Prompt gamma rays of ^{57}Fe

This work				From Demidov Atlas [10]		I_R (this work)/I_R (Demidov)
$E\gamma$ (keV)	$P_{E\gamma}(90°)/\varepsilon_{E\gamma}$ ($\times 10^{-8}$) (count)	I_R (relative) (%)	$\langle\sigma_{E\gamma}(90°)\rangle$ (mb)	$E\gamma$ (keV)	I_R (relative) (%)	
121.84 ± 0.05	3.63 ± 0.24	1.28 ± 0.11	324 ± 24	122.1 ± 0.2	2.2 ± 0.2	0.58 ± 0.07
136.33 ± 0.08	0.36 ± 0.08	0.13 ± 0.03	32 ± 7	–	–	–
211.7 ± 0.1	0.29 ± 0.07	0.10 ± 0.02	26 ± 6	–	–	–
230.25 ± 0.07	0.26 ± 0.05	0.09 ± 0.02	23 ± 4	–	–	–
352.13 ± 0.04	2.81 ± 0.35	0.99 ± 0.14	251 ± 32	352.5 ± 0.0	1.6 ± 0.2	0.62 ± 0.12
366.48 ± 0.08	0.89 ± 0.14	0.31 ± 0.05	79 ± 13	367.1 ± 0.2	0.54 ± 0.05	0.57 ± 0.18
650.65 ± 0.08	0.46 ± 0.05	0.16 ± 0.02	41 ± 5	–	–	–
870.75 ± 0.06	0.96 ± 0.08	0.34 ± 0.03	85 ± 8	–	–	–
992.5 ± 0.1	0.24 ± 0.06	0.08 ± 0.02	22 ± 5	992.8 ± 0.4	0.10 ± 0.03	0.80 ± 0.31
1298.9 ± 0.1	0.20 ± 0.11	0.07 ± 0.04	18 ± 10	1298.9 ± 0.4^a	0.12 ± 0.04	0.58 ± 0.38
1412.4 ± 0.2	0.15 ± 0.05	0.05 ± 0.02	14 ± 4	–	–	–
1814.0 ± 0.2	0.58 ± 0.08	0.20 ± 0.03	52 ± 8	–	–	–

$E\gamma$ is the gamma-ray energy, $P_{E\gamma}(90°)/\varepsilon_{E\gamma}$ the net count in the gamma ray peak divided by the full-energy-peak efficiency, I_R the relative intensity of the gamma ray and $\langle\sigma_{E\gamma}(90°)\rangle$ the fast neutron spectrum averaged isotopic cross section for gamma ray production at angle of 90° between neutron beam and detector determined with Eq. (2)

Possible interference from [a] the 1303 keV line of ^{56}Fe

cases. The intensities of the gamma rays were calculated relative to the 847-keV line of ^{56}Fe (100%), and they are given with the values determined in [10] in Tables 2, 3 and 4. The ratios of the intensities are given in the last column of the tables. The average value of the ratios is 0.85 ± 0.26. For 25 gamma rays, the half of the data, the intensities agree well with each other taking into account their uncertainties. For the remaining gamma rays the intensities listed in Demidov Atlas are higher by factors ranging from 1.5 to 2.5 without following any trend according to the energy of the gamma rays. The cause for these high values may probably be due to the presence of the 5 cm thick iron plate in front

Table 4 Prompt gamma rays of ^{54}Fe and ^{58}Fe

This work				Demidov Atlas [10]		I_R (this work)/I_R (Demidov)
$E\gamma$ (keV)	$P_{E\gamma}(90°)/\varepsilon_{E\gamma}$ ($\times 10^{-8}$) (count)	I_R (relative) (%)	$\langle\sigma_{E\gamma}(90°)\rangle$ (mb)	$E\gamma$ (keV)	I_R (relative) (%)	
757.6 ± 0.2	0.18 ± 0.4	0.06 ± 0.01	6 ± 1	757.3 ± 0.4	0.10 ± 0.03	0.60 ± 0.21
1130.46 ± 0.06	1.06 ± 0.08	0.37 ± 0.04	34 ± 3	1130.0 ± 0.3	0.39 ± 0.04	0.95 ± 0.14
1153.18 ± 0.09	0.42 ± 0.04	0.15 ± 0.02	13 ± 1	1152.8 ± 0.4	0.14 ± 0.03	1.07 ± 0.27
1408.32 ± 0.05	9.92 ± 0.58	3.49 ± 0.29	321 ± 22	1408.2 ± 0.2	3.5 ± 0.2	1.00 ± 0.10
1509.7 ± 0.3	0.23 ± 0.04	0.08 ± 0.02	0.49 ± 0.09	1509.7 ± 0.10	0.08 ± 0.03	1.00 ± 0.53
1550.47 ± 0.04	0.45 ± 0.08	0.16 ± 0.03	14 ± 3	1551.2 ± 0.4	0.25 ± 0.05	0.64 ± 0.18
1937.0 ± 0.2	0.29 ± 0.03	0.10 ± 0.01	9 ± 1	–	–	–
3095.4 ± 0.6	0.20 ± 0.04	0.07 ± 0.02	6 ± 1	–	–	–
3166.6 ± 0.2	0.37 ± 0.06	0.13 ± 0.02	12 ± 2	–	–	–
810.67 ± 0.07[a]	1.17 ± 0.19	0.41 ± 0.07	786 ± 130	810.3 ± 0.02	0.43 ± 0.03	0.95 ± 0.17

$E\gamma$ is the gamma-ray energy, $P_{E\gamma}(90°)/\varepsilon_{E\gamma}$ the net count in the gamma ray peak divided by the full-energy-peak efficiency, I_R the relative intensity of the gamma ray and $\langle\sigma_{E\gamma}(90°)\rangle$ the fast neutron spectrum averaged isotopic cross section for gamma ray production at angle of 90° between neutron beam and detector determined with Eq. (2)

[a]Gamma-ray of ^{58}Fe

of the shielding of the Demidov´s spectrometer as prompt gamma rays of iron are also visible in many spectra of the Demidov Atlas.

The net peak area of a prompt gamma ray of energy $E\gamma$ measured at the angle of 90° between neutron beam and detector, $P_{E\gamma}(90°)$, may be expressed by the following equation:

$$P_{E\gamma}(90°) = \frac{m}{M} \cdot N_A \cdot h \cdot \varepsilon_{E\gamma} \cdot \sigma_{E\gamma}(90°) \cdot \Phi \cdot t_c \quad (2)$$

where m (g) is the amount of element, M (g mol^{-1}) the molar mass of the element, N_A the Avogadro number, h the abundance of the isotope considered, Φ (cm^{-2} s^{-1}) the integral fast neutron flux at sample position, t_c (s) the counting (live) time, $\varepsilon_{E\gamma}$ the full energy peak efficiency previously determined in [11] with the same gamma-ray collimation (6 cm diameter opening). $\sigma_{E\gamma}(90°)$ is the fast neutron spectrum averaged isotopic cross section for gamma ray production which may be given also by:

$$\sigma_{E\gamma}(90°) = \frac{\int_{Emin}^{Emax} \sigma_{E\gamma}(90°, E) \cdot \varphi(E) \cdot dE}{\int_{Emin}^{Emax} \varphi(E) \cdot dE} \quad (3)$$

where $\varphi(E)$ is the differential neutron flux density and $\sigma_{E\gamma}(90°, E)$ the isotopic cross section for gamma ray production at the corresponding neutron energy E. The values of $\sigma_{E\gamma}(90°)$ deduced by means of Eq. (2) are given in Tables 2, 3 and 4. Corrections for neutron absorption and multiple scattering and for gamma absorption were neglected since the iron foil is very thin.

To check the validity of the results, the values of $\sigma_{E\gamma}(90°)$ were calculated for the strongest ^{56}Fe

gamma-rays at 847, 1238 and 1810 keV using as reference their gamma-ray production cross sections measured for several discrete incident neutron energies at an angle of 125° by Dickens et al. [20]. These values are listed together with the corresponding neutron energy bins in Table 5. According to [21] we can write:

$$\sigma_{E\gamma}(90°, E_i) = \sigma_{E\gamma}(125°, E_i) \cdot \left[\frac{W_{E\gamma}(125°, E_i)}{W_{E\gamma}(90°, E_i)}\right]^{-1} \quad (4)$$

where $\sigma_{E\gamma}(\theta, E_i)$ is the isotopic cross section for gamma-ray production determined at the angle θ between neutron beam and detector axis for an incident neutron energy E_i and $W_{E\gamma}(\theta, E_i)$ the corresponding angular distribution factor. For gamma rays induced by inelastic scattering of neutrons the angular distribution factor is described quite accurately by the first even terms of the Legendre polynomial [23]:

$$W_{E\gamma}(\theta, E_i) = 1 + a_2(E\gamma, E_i) \cdot P_2(\cos\theta) + a_4(E\gamma, E_i) \cdot P_4(\cos\theta) \quad (5)$$

with

$$P_2(\cos\theta) = \frac{1}{2} \cdot \left[3 \cdot (\cos\theta)^2 - 1\right] \quad (6)$$

and

$$P_4(\cos\theta) = \frac{1}{8} \cdot \left[35 \cdot (\cos\theta)^4 - 30 \cdot (\cos\theta)^2 + 3\right] \quad (7)$$

In the case of the 847 keV gamma ray the coefficients a_2 and a_4 were taken in [22] for neutron energies lower than 2 MeV and read out from the figure 2 of Ref. [23]

Table 5 Data for calculation of the fast neutron spectrum averaged cross section $\langle \sigma_{E\gamma}(90°)\rangle$ for production of the gamma rays at 846.8, 1238.3 and 1810.8 keV of ^{56}Fe by means of Eq. (8)

Ei (MeV)	$\Phi(Ei)$ (cm^{-2} s^{-1})	$E\gamma=846.8$ keV			$E\gamma=1238.3$ keV			$E\gamma=1810.8$ keV		
		$\sigma_{E\gamma}(125°, Ei)$ (mb)	$W(125°, Ei)/W(90°, Ei)$	$\sigma_{E\gamma}(90°, Ei)$ (mb)	$\sigma_{E\gamma}(125°, Ei)$ (mb)	$W(125°, Ei)/W(90°, Ei)$	$\sigma_{E\gamma}(90°, Ei)$ (mb)	$\sigma_{E\gamma}(125°, Ei)$ (mb)	$W(125°, Ei)/W(90°, Ei)$	$\sigma_{E\gamma}(90°, Ei)$ (mb)
0.86–0.91	2.73 10^6	164 (40)	2.31 (24)	71 (19)						
0.91–0.98	3.82 10^6	275 (52)	2.02 (24)	136 (30)						
0.98–1.16	8.37 10^6	470 (49)	1.70 (8)	276 (32)						
1.16–1.68	1.98 10^7	652 (37)	1.37 (5)	474 (32)						
1.68–2.36	2.52 10^7	810 (55)	1.21 (6)	667 (56)	13 (2)^a	1.23 (6)	11 (1)			
2.36–3.07	2.01 10^7	961 (58)	1.15 (6)	838 (66)	73 (5)	1.20 (6)	61 (4)	83 (8)^b	1.19 (6)	69 (8)
3.07–3.83	1.37 10^7	1115 (77)	1.11 (6)	1001 (86)	162 (12)	1.18 (6)	138 (10)	167 (13)	1.16 (6)	144 (13)
3.83–4.71	8.43 10^6	1180 (62)	1.09 (5)	1079 (78)	239 (13)	1.15 (6)	207 (11)	144 (8)	1.12 (6)	128 (10)
4.71–5.65	4.53 10^6	1274 (57)	1.08 (5)	1178 (79)	310 (14)	1.14 (6)	272 (12)	154 (9)	1.10 (5)	140 (10)
5.65–6.56	2.29 10^6	1331 (90)	1.07 (5)	1239 (104)	400 (30)	1.13 (6)	355 (26)	152 (10)	1.08 (5)	140 (11)
6.56–7.49	1.38 10^6	1255 (79)	1.07 (5)	1173 (94)	402 (26)	1.12 (5)	360 (24)	135 (10)	1.07 (5)	126 (11)
7.49–8.26	6.96 10^5	1160 (79)	1.07 (5)	1086 (92)	421 (28)	1.11 (5)	379 (25)	115 (9)	1.06 (5)	110 (8)
8.26–9.02	4.38 10^5	1131 (75)	1.07 (5)	1060 (88)	444 (31)	1.10 (5)	401 (28)	111 (9)	1.06 (5)	105 (10)
9.02–9.90	3.02 10^5	1131 (72)	1.07 (5)	1061 (86)	469 (32)	1.10 (5)	426 (29)	106 (8)	1.05 (5)	101 (9)
9.90–10.56	1.05 10^5	1123 (72)	1.07 (5)	1053 (85)	520 (36)	1.10 (5)	473 (33)	100 (9)	1.05 (5)	95 (10)
10.56–11.28	1.07 10^5	1171 (52)	1.07 (5)	1097 (73)	499 (23)	1.10 (5)	456 (21)	97 (4)	1.05 (5)	92 (8)
11.28–12.09	7.20 10^4	1101 (54)	1.07 (5)	1031 (72)	511 (26)	1.09 (5)	468 (24)	91 (7)	1.04 (5)	87 (8)
12.09–12.98	4.23 10^4	947 (41)	1.07 (5)	886 (59)	490 (21)	1.09 (5)	449 (19)	81 (7)	1.04 (5)	77 (7)
12.98–13.97	2.40 10^4	774 (35)	1.07 (5)	723 (49)	431 (18)	1.09 (5)	396 (16)	55 (5)	1.04 (5)	50 (6)
13.97–15.09	1.30 10^4	621 (29)	1.07 (5)	579 (39)	290 (16)	1.08 (5)	267 (15)	37 (5)	1.04 (5)	36 (5)
15.09–16.69	7.32 10^3	409 (25)	1.07 (5)	380 (30)	193 (14)	1.08 (5)	178 (13)	31 (4)	1.03 (5)	30 (4)
16.69–18.55	2.74 10^3	293 (16)	1.08 (5)	271 (21)	126.6 (8)	1.08 (5)	117 (7)	21 (4)	1.03 (5)	20 (4)
18.55–20.76	5.16 10^2	249 (11)	1.08 (5)	229 (15)	96.6 (6)	1.08 (5)	90 (5)	10 (3)	1.03 (5)	10 (3)
Neutron spectrum averaged cross section $\sigma_{E\gamma}(90°)$				576 (75)			59 (6)			35 (5)

The gamma-ray production cross sections $\sigma_{E\gamma}(125°, Ei)$ measured at 125° for the incident neutron energy Ei are taken in [20]. $\Phi(Ei)$ is the neutron flux in the neutron energy bin i calculated from the neutron spectrum measured in this work. The other quantities are given in the text

^{a} For neutron energy bin $2.12 \leq En \leq 2.236$; $\Phi(Ei) = 8.50 \times 10^6$ cm^{-2} s^{-1}

^{b} For neutron energy bin $3.01 \leq En \leq 3.07$; $\Phi(Ei) = 1.36 \times 10^5$ cm^{-2} s^{-1}

for higher neutron energies up to 14 MeV. For the gamma rays at 1238 and 1810 keV the coefficients a_2 were read out from the figure 2 of Ref. [23] and the coefficients a_4 being very small were assumed to be zero [23]. This assumption implies uncertainties less than 0.5 to 2% for the angular distribution factors depending on the ratio between a_2 and a_4. The neutron energy dependence of the ratio $W_{E_\gamma}(125°, E_i)/W_{E_\gamma}(90°, E_i)$ is shown for the aforementioned gamma-rays in Fig. 7. Analytical expressions were obtained by fitting the data with appropriate rational functions (solid lines in Fig. 7). As shown in Figs. 8 and 9, respectively, the ratios $W_{E_\gamma}(125°, E_i)/W_{E_\gamma}(90°, E_i)$ calculated for the 847 keV gamma ray and with the incident neutron energies between 0.95 and 4 MeV and for the 1238 and 1810 keV gamma rays at neutron energy of 4 MeV, respectively, agree well with the experimental values given in [24]. Thus, the method used in this work to evaluate the angular distribution factors of the gamma rays is consistent. The ratios $W_{E_\gamma}(125°, E_i)/W_{E_\gamma}(90°, E_i)$ as well as the values $<\sigma_{E_\gamma}(90°, E_i)>$ calculated by means of relation (4) using the cross sections measured at 125° [20] are given in Table 5. It is interesting to note the convergence of the angular-distribution correction factors for the different types of radiation fields, the 847 and 1238 keV gammas being stretched quadrupole E2 transitions while the 1811 keV gamma is a mixed M1+E2 transition with a gamma-ray multipole mixing ratio of −0.18 [26].

The neutron spectrum averaged isotopic cross section for gamma-ray production was calculated with Eq. (8) which is an approximation for relation (3).

$$\langle \sigma_{E_\gamma}(90°) \rangle = \frac{\sum_i \sigma_{E_\gamma}(90°, E_i) \cdot \Phi(E_i)}{\Phi} \quad (8)$$

where $\Phi(E_i)$ is the neutron flux in the neutron energy bin i calculated from the neutron spectrum measured in this work (column 2 of Table 5) and Φ the fast neutron flux. The values of $\sigma_{E_\gamma}(90°)$ obtained with Eq. (8), are: 576 ± 75 mb, 59 ± 6 mb and 35 ± 5 mb for the gamma-rays at 847, 1238 and 1810, keV respectively. These values agree well with the experimental values calculated with Eq. (2), 586 ± 41 mb, 58 ± 5 mb and 37 ± 3 mb. Thus, we can assume that the neutron spectrum averaged isotopic cross sections for the production of the others iron prompt gamma rays detected in this work are reliable.

Conclusions

Prompt gamma-ray emission induced by inelastic scattering of fission neutrons on iron was measured with the FaNGaS instrument operated at MLZ. The measurements were performed at an angle of 90° between the neutron beam and the detector with a fast neutron flux of 1.40×10^8 cm^{-2} s^{-1} at sample position. A total of 81 prompt gamma rays were detected and their relative intensities (using the 847 keV gamma-ray of ^{56}Fe as reference) and fast neutron spectrum averaged production cross sections were determined. Compared to the work of Demidov et al. [10], 33 gamma lines were detected additionally. We also found out that 11 gamma lines were wrongly assigned

Fig. 7 Neutron energy dependence of the ratio of the angular distribution factors for the three strongest rays of ^{56}Fe. The solid lines represent the fit of the data with following rational functions: $(a+b\times E_i)/(1+c\times E_i + d\times E_i^2)$ for the 847 keV gamma line with $a=0.5984$, $b=−1.4842$, $c=−1.4835$ and $d=0.0048$; $(a+b\times E_i)/(1+c\times E_i)$ for the 1238 keV gamma line with $a=2.0779$, $b=2.778$ and $c=2.1619$; $(a+b\times E_i)/(1+c\times E_i)$ for the 1810 keV gamma line with $a=−1.1930$, $b=1.3856$ and $c=−1.1786$
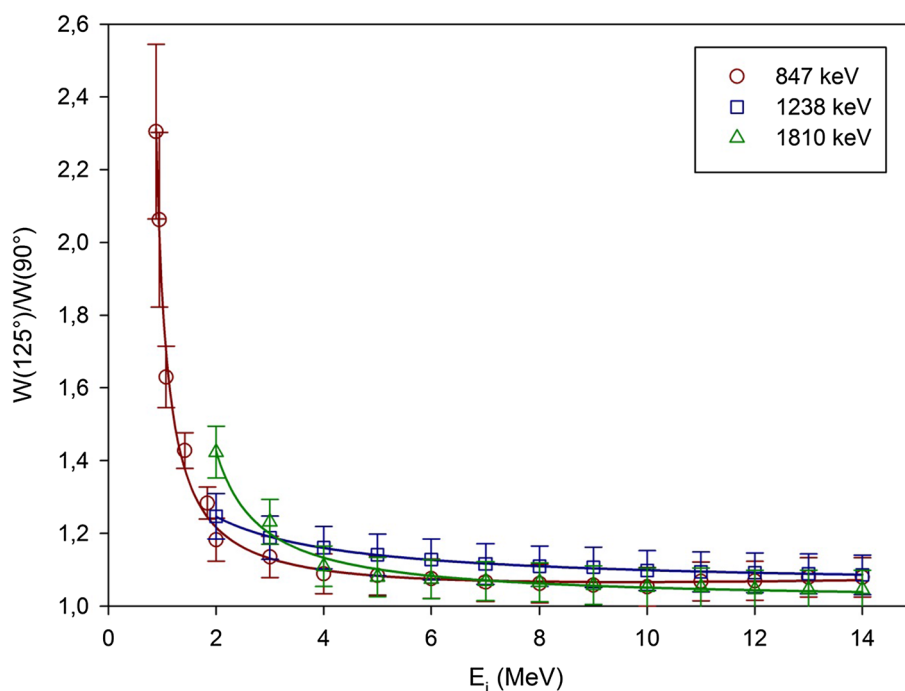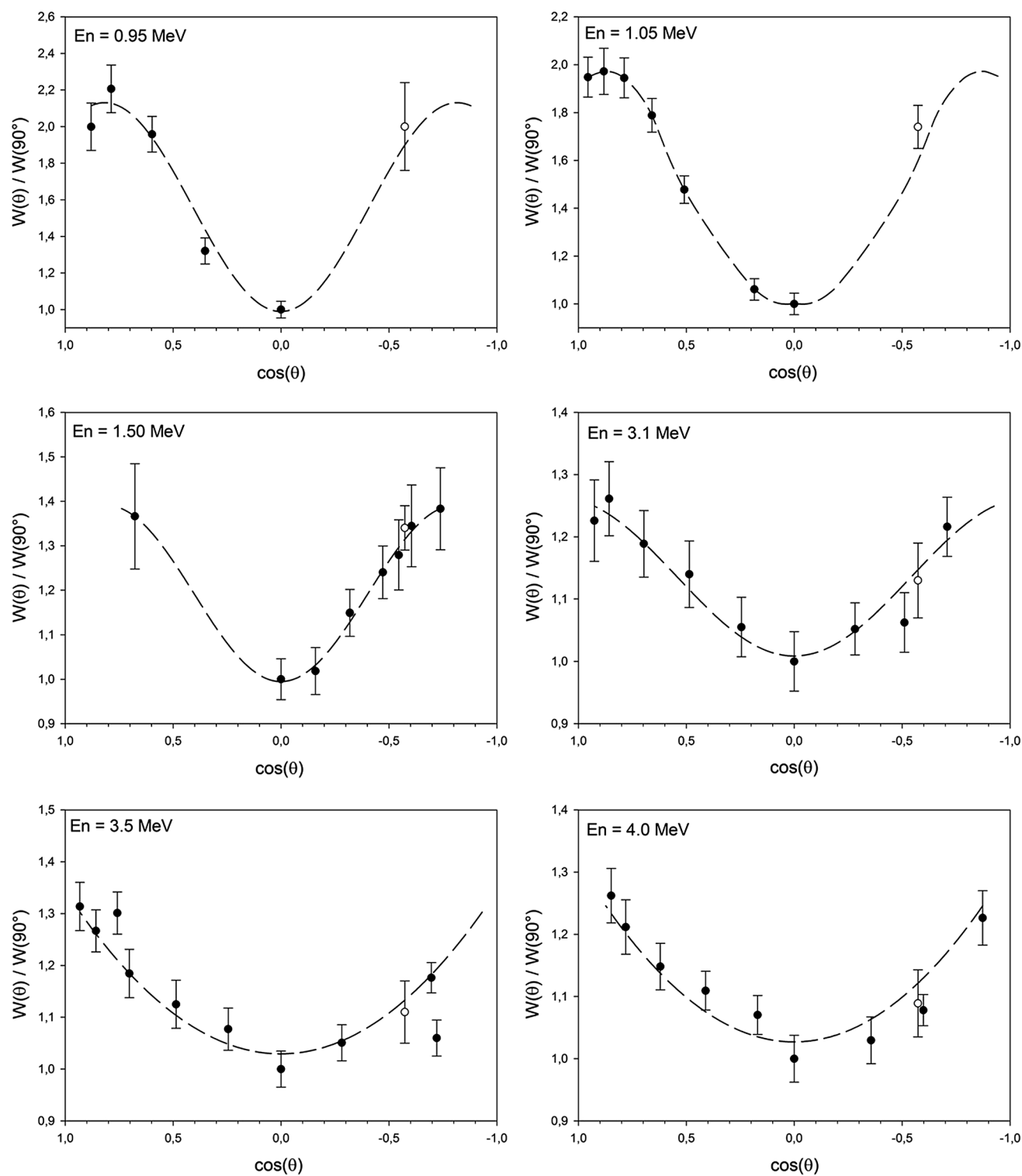
Fig. 8 Relative angular distributions for the 847 keV gamma ray experimentally determined at several incident neutron energies (close symbols) [24] and value calculated in this work for $\theta = 125°$ (open symbols). The dashed lines are fits of the data with a sinus function and serve as a guide to the eye
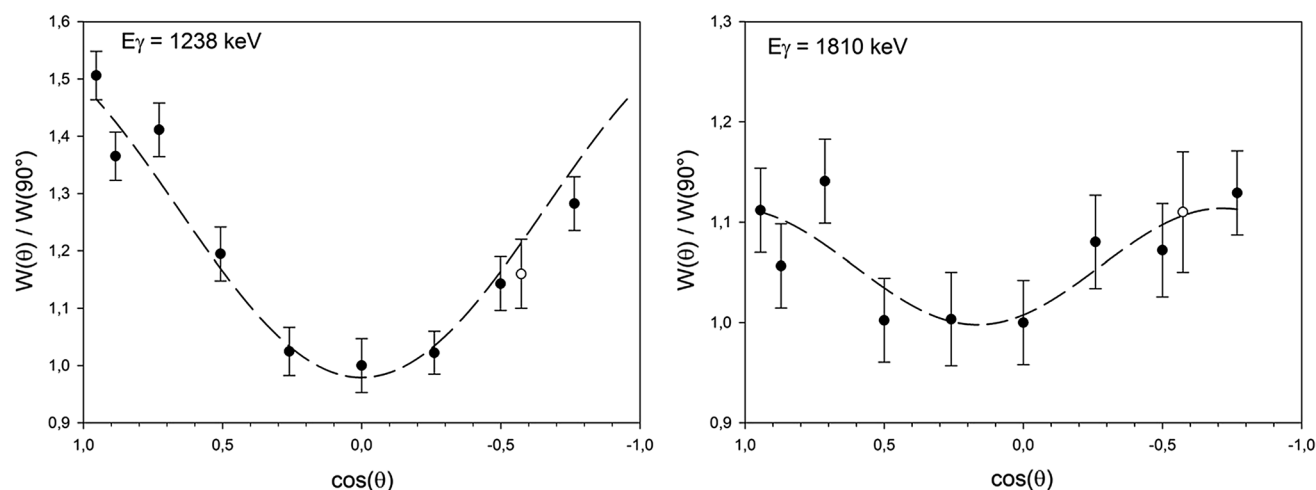
Fig. 9 Relative angular distributions for 1238 and 1811 keV gamma rays experimentally determined at an incident neutron energy of 4 MeV (close symbols) [24] and value calculated in this work for $\theta = 125°$ (open symbols). The dashed lines are fits of the data with a sinus function and serve as a guide to the eye

to iron in the Demidov Atlas. For only the half of the gamma rays observed in both works, the intensities agree well with each other considering their uncertainties. For the remaining gamma rays the intensities listed in Demidov Atlas are largely higher probably due the presence of iron in the shielding of the Demidov´s spectrometer. Additionally, the reliability of the gamma-ray production cross sections measured at 90° was demonstrated from the gamma rays at 847, 1238 and 1810 keV by convoluting their discrete-energy gamma-ray production cross sections obtained at 125° [20] with the fast neutron spectrum delivered at the sample position and taking into account angular correlation factors. Thus, the FaNGaS instrument proved to be a suitable tool to investigate fast neutron induced prompt gamma-ray emission to create a comprehensive data catalogue on (n,n′γ) reactions and to perform chemical analysis of large samples or small samples complementary to PGNAA with cold neutrons as well.

References

1. Molnár GL (2004) Handbook of prompt gamma activation analysis with neutron beams. Kluwer Academic Publishers ISBN 1-4020-1304-3
2. Sueki K, Kobayashi K, Sato W, Nakahara H, Tomizawa T (1996) Nondestructive determination of major elements in a large sample by prompt gamma ray neutron activation analysis. Anal Chem 68:2203–2209
3. Degenaar LH, Blaauw M, Bode P, de Goeij JJM (2004) Validation of MCNP for large sample thermal-beam prompt-gamma neutron activation analysis. J Radioanal Nucl Chem 2:311–315
4. Blaauw M, Degenaar LH, de Goeij JJM (2007) Development of a non-invasive method for the determination of the macroscopic neutron cross sections of a sample matrix in large-sample prompt-gamma neutron activation analysis. J Radioanal Nucl Chem 3:765–770
5. Blaauw M, Belgya T (2005) Neutron self-shielding correction for prompt gamma neutron activation analysis of large samples. J Radioanal Nucl Chem 265:257–259
6. Schrader CD, Stinner RJ (1961) Remote analysis of surfaces by neutron-gamma-ray inelastic scattering techniques. J Geophys Res 66:1951–1956
7. Jiggins AH, Habbani FI (1976) Prompt gamma-ray analysis using 3.29 MeV neutron inelastic scattering. Int J Appl Radiat Isot 27:689–693
8. Yates SW, Filo AJ, Cheng CY, Coope DF (1978) Elemental analysis by gamma detection following inelastic neutron scattering. J Radional Nucl Chem 46:343–355
9. Sowerby BD (1979) Elemental analysis by neutron inelastic scatter gamma rays with a radioisotope neutron source. Nucl Instrum Methods 166:571–579
10. Demidov A, Govor L, Cherepantsev M, Ahmed S, Al-Najiar M, Al-Amili N, Al-Assafi N, Rammo N (1978) Atlas of gamma-ray spectra from the inelastic scattering of reactor fast neutrons. Atomizdat, Moscow
11. Randriamalala TH, Rossbach M, Mauerhofer E, Zs Révay, Söllrad S, Wagner FM (2016) FaNGaS: a new instrument for (n, n′, γ) reaction measurements at FRM II. Nucl Instrum Methods A806:370–377

12. Rossbach M, Randriamalala T, Mauerhofer E, Zs Révay, Söllrad S (2016) Prompt and delayed inelastic scattering from fission neutron irradiation—first results of FaNGas. J Radioanal Nucl Chem 309:149–154

13. Wagner FM, Kneschaurek P, Kastenmüller A, Loeper-Kabasakal B, Kampfer S, Breitkreutz H, Waschowski W, Molls M, Petry W (2008) The Munich fission neutron therapy facility MEDAPP at the research reactor FRM II. Strahlenther Onkol 184:643–646

14. Mühlbauer MJ, Büchert T, Kellermeier M, Knapp M, Makowska M, Schulz M, Zimmik S, Ehrenberg H (2018) Neutron imaging with fission and thermal neutrons at NECTAR at MLZ. Physica B 551:359–363

15. Zs Révay, Belgya T, Molnár GL (2005) Application of Hypermet-PC in PGAA. J Radioanal Nucl Chem 265:261–265

16. International Atomic Energy Agency. Codes for radiation damage calculations and neutron spectral adjustment. http://www-nds.iaea.org/irdf2002/codes/index.htmlx

17. Perey FG (1977) Least-squares dosimetry unfolding: the program STAY'SL. ORNL/TM-6062, Oak Ridge National Laboratory, Oak Ridge, Tennessee

18. OECD NEA Data Bank, JANIS Book of neutron-induced cross-sections (2018). https://www.oecd-nea.org/janis/book/book-neutron-2018-05.pdf

19. NuDat 2.8 National Nuclear Data Center, Brookhaven National Laboratory. https://www.nndc.bnl.gov/nudat2/

20. Dickens JK, Todd JH, Larson DC (1990) Cross section for production of 70 discrete—energy gamma rays created by neutron interactions with ^{56}Fe for En to 40 MeV: tabulated data. Report ORNL/TM-11671

21. Dietz M, Bemmerer D, Beyer R, Gohl S, Junghans AR, Kögler R, Massarczyk R, Müller SE, Schmidt K, Schwengner R, Szücs T, Takacs MP, Wagner A, Wagner L (2017) Angular distribution measurement of gamma rays from in inelastic neutron scattering on ^{56}Fe at the nELBE time-of-flight facility. In: EPJ Web of conferences, vol 146, p 11040

22. Dietz M (2016) Determination of the γ-ray-angular distribution in the inelastic scattering of fast neutrons on ^{56}Fe at nELBE. Master Thesis, Technische Universität Dresden, Germany. https://www.hzdr.de/publications/PublDoc-11136.pdf

23. Savin MV, Livke AV, YuYa Nefedov, Shvestsov MS, Zvenigorodskii AG, Blokhin AI (2000) Evaluation of angular distributions and gamma-rays production cross section for iron. J Nucl Sci Technol 37(Supplement 1):748–752

24. Benjamin RW, Buchanan PS, Morgan IL (1966) Gamma rays produced in the 56Fe(n, n′γ)56Fe reaction. Nucl Phys 79:241–256

25. Erdtmann G (1976) Neutron activation tables. Verlag Chemie, Weinheim

26. Bradley DI, Stone NJ, Rikovska J, Novakova D, Ferencei J (1986) Level spins and transition multipolarities in ^{56}Fe studied by nuclear orientation of ^{56}Co. J Phys G Nucl Phys 12:115–128